Treatment of artificial pharmaceutical wastewater containing amoxicillin by a sequential electrocoagulation with calcium salt followed by nanofiltration

A. Oulebsir, T. Chaabane, H. Tounsi, K. Omine, V. Sivasankar, A. Flilissa, A. Darchen

Treatment of artificial pharmaceutical wastewater containing amoxicillin by a sequential electrocoagulation with calcium salt followed by nanofiltration

Aimad Oulebsir[1], Toufik Chaabane[1]*, Hanane Tounsi[1], Kiyoshi Omine[2], Venkataraman Sivasankar[3]*, Abdenacer Flilissa[4], André Darchen[5]

[1] Reaction Engineering Laboratory, Faculty of Mechanical and Process Engineering (FGMGP)/Environmental Department, University of Science and Technology Houari Boumédiène (USTHB), P 32 El-Alia
16111, Bab Ezzouar, Algiers, Algeria.

[2] Department of Civil Engineering, School of Engineering, Nagasaki University, 1-14 Bunkyo-machi Nagasaki 8528521, Japan.

[3] P.G. and Research Department of Chemistry, Pachaiyappa's College, Chennai 600 030, Tamil Nadu, India.

[4] Laboratoire MCGN, Département de Pharmacie, Faculté de Médecine, Université Ferhat Abbas, Sétif-1, 19000, Algeria

[5] UMR CNRS n°6226 Institut des Sciences Chimiques de Rennes, ENSCR, 11, Allée de Beaulieu, CS 50837, 35708 Rennes Cedex 7, France.

* Corresponding authors

E-mail addresses: tchaabane@usthb.dz; tfkchaabane@yahoo.fr (T. Chaabane) and sivshri.20@gmail.com (V. Sivasankar)

Graphical abstract

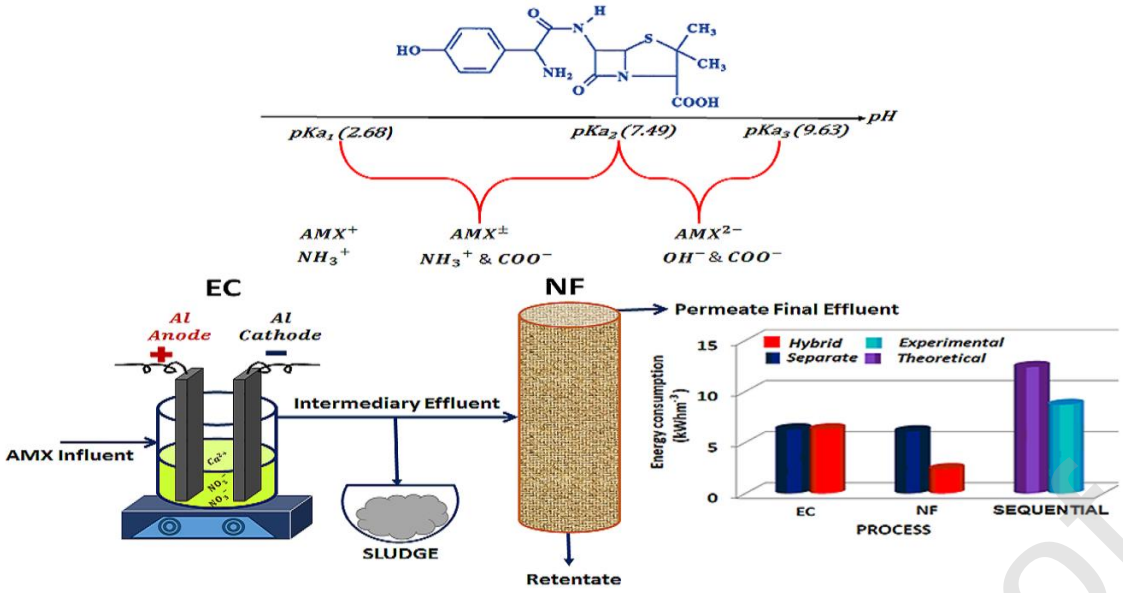

Research highlights

- AMX removal of 99% was obtained in EC – NF hybrid process
- The electrical consumption was reduced by 30% in the sequential process
- Calcium ions are involved in the electrogenerated solids
- The EC pre-treated feed ensured the prolonged life of NF membrane

Abstract

The present study deals with the treatment of an artificial pharmaceutical waste which contained amoxicillin (AMX) by using successively an electrocoagulation (EC) with $Ca(NO_3)_2$ as an electrolyte and a nanofiltration (NF) with a Nanomax-50 membrane. The effect of the current intensity and of the operating pressure was investigated for separately EC and NF, respectively. The AMX removal as a function of pH and initial AMX concentration was also investigated for the separately conducted EC and NF processes. The best percentage removal of AMX by EC and NF was recorded to be 52.7% and 99.0%, respectively. In the case of the sequential processes EC followed by NF, the removal of AMX was 98.2% and

97.5% at pH 2.5 and 10, respectively. The contribution of both EC and NF towards the AMX removal efficiency in the case of the sequential process was very much significant. It is remarkable that the EC pre-treated feed into NF was explored with several benefits such as high removal efficiency, calcium involved in EC process, prolonged membrane life and reduced power consumption. The electrogenerated solids (the sediment and the cathode deposit) were characterized using Fourier Transform Infra-red spectroscopy (FTIR), Energy Dispersive Spectroscopy (EDS) coupled to Scanning Electron Microscopy (SEM), X-ray Photoelectron Spectroscopy (XPS) and Thermo Gravimetry Analysis (TGA). It appeared that calcium was involved in the electrogenerated solids. It gave a cathode deposit of $Ca(OH)_2$ in which some AMX was embedded.

Key words: *Sequential processes; Electrocoagulation; Calcium electrolyte; Nanofiltration; Amoxicillin; Sludge characterization*

1. Introduction

Pharmaceuticals belong to a category of emerging pollutants which has been the subject of much concerns in environmental engineering all around the world [1,2]. Numerous studies have been developed aiming at their removal from industrial and municipal waste waters [3,4]. Numerous reviews bring together removal technologies which use membrane processes [5], electrochemical degradation [6], Fenton process [7], adsorption [8], biological treatments [9], or various combined technologies [10-13]. In addition to the fact that these treatments aim to eliminate in the effluents hazardous compounds, even at low concentration, these treatments also aim at recycling or reuse industrial waters, or a reduction of their toxicity with the perspective of a biological treatment.

Many processes have been carried out for the antibiotic removals. Regarding amoxicillin (AMX), which is a β-lactam antibiotic frequently analyzed in wastewaters, its removal has been investigated by single process such as adsorption [14-16], Fenton oxidation [17,18], oxidative degradation [19,20] extraction [21], photocatalysis [22] and membrane separation [23-25]. Combined technologies, sometimes called hybrid processes, have also been developed in order to improve removal capacities. In wastewater, amoxicillin elimination has been investigated for a combination of ultrasound and ozone oxidation [26], combined Fenton process [27,28], adsorption and ozone oxidation [29], electrocoagulation as single or in combined processes has been applied to the amoxicillin removal [30-33], but never coupled to a membrane separation. “Energy consumption of nanofiltration processes is deleteriously impacted by the unavoidable membrane fouling [34]. Electrocoagulation is known to have a positive effect in mitigation of biofouling [35,36]. In a first intention, a calcium salt was used in order to improve the formation of adsorbent materials. Since all the calcium ions are not totally consumed during EC, it is not excluded that the residual calcium has also a positive effect in mitigation of biofouling [37-39].”

In the present work, the sequential treatment of electrocoagulation followed by a nanofiltration separation was applied to the removal of high concentration of amoxicillin from synthetic water. This study was carried out with a triple objective, to simulate the treatment of washing water arising from industrial equipment, protect the nanofiltration membrane for its fouling, and investigate the use of calcium salt in the electrocoagulation process.

2. Materials and methods

2.1. Chemicals

All the chemicals and reagents used in the study were of Analar grade. Amoxicillin ($C_{16}H_{19}N_3O_5S$; Mol. Wt. 365.4 g mol^{-1}) was purchased from GlaskoSmithKline (Germany) and the electrolyte $Ca(NO_3)_2.4H_2O$ was purchased from Biochem (Canada). NaOH and HCl were purchased from Sigma-Aldrich (France). All the solutions were made with distilled water. Aluminum of electrodes was grade 1050A of the registered international designation purchased from Ridings and Dafrodis (Bouc-Bel-Air, France).

2.2. Electrocoagulation (EC) process

2.2.1. Electrocoagulation cell assembly

Electrodes were aluminum plates of 11.9 cm × 4.7 cm × 0.4 cm dimensions. Prior to electrolysis, the electrodes were immersed in 0.1 M NaOH for 10 min, then they were rinsed with distilled water and finally they were dried in an oven at 105°C for1 h. The electrolyses were carried out in batch reactor, under magnetic stirring. The electrodes were connected to a digital DC supply (2303 GPS-type) with voltage and current range of 0 – 32 V and 0 – 4 A, respectively. A digital ammeter and voltmeter were used to measure the current and the voltage. pH adjustments during the experiments were done with HCl (0.1 M) or NaOH (0.1 M) using pH meter (model Sartorius).

2.2.2. Instrumental characterization

At the end of each electrolysis the residual AMX concentration was determined by UV Spectrophotometry (Model Shimadzu 1800) at the absorbance wavelength of 246 nm, after 24 h of decantation. Beside residual AMX, no degradation compounds were detected by this analysis. The filtered sludge and the cathode deposit were examined using Field Emission Scanning Electron Microscopy (FE – SEM) with JEOL JSM – 7500 FAM and JEOL EDS JSM – 7500 equipped with FA View (JEOL) software. The structural characterization of the materials was investigated by powder X – Ray Diffraction (XRD) using Rigaku MiniFlex 600 operated at 40 kV and 15 mA and the phase identification was performed with the PDXL2 (Rigaku) software. The functional group identification was done by Fourier Transform Infra-Red (FTIR) using ThermoNicolet Nexus 670 NT FTIR equipped with the Attenuated Total Reflectance (ATR) equipment. The Thermo Gravimetric Analyses (TGA) were performed as described in [40] with a thermo gravimetric analyzer (TG: Shimadzu: TGA – 50H). XPS analyses were performed using KRATOS Axis Ultra DLD (Kratos Analytical, Manchester, United Kingdom). An incident monochromatic X-ray beam from the Al target (15 kV, 10 mA) was focused on a 0.7 mm × 0.3 mm area of the sample surface at an angle of 45˚ to the sample surface. The electron energy analyzer (located perpendicular to the sample surface) was operated with pass energy of 20 eV enabling high resolution of the spectra to be obtained. The step size of 0.02 eV was employed and each peak was scanned twice. The surface contamination was commonly removed by the sputtering technique using Ar^+ ion bombardment.

2.3. Nano-Filtration (NF) process

The membrane used in nanofiltration was the Nanomax-50 supplied by Millipore. It was constituted with three layers of polyamide and polysulfone. The NF membrane had a surface area of 0.37 m^2 and a molecular weight cut-off of 300 Dalton, with a pore diameter of

1 nm. It supported a maximum temperature of 40°C and a pressure of 2.8 MPa. Its hydraulic permeability was found to be 2.21×10^{-11} m $s^{-1}Pa^{-1}$. After each experiment, a cleaning was carried out by using distilled water to remove the fouling elements from the membrane and the pipes.

The NF equipment is presented in Fig. 1, with a volumetric pump, a feed tank of 12 L capacity, two pressure regulation valves, two pressure sensors, a filtration module that can accommodate spiral membranes with a diameter of 4.54×10^{-2} m and a length of 30.5×10^{-2} m. The experiments were carried out with 6 L of AMX solution of each concentration (10 mg L^{-1}, 25 mg L^{-1}, 50 mg L^{-1}, 100 mg L^{-1} and 150 mg L^{-1}) at pH 2.5 or 10 and the operating pressure between 0.1 MPa and 0.5 MPa at the room temperature. The permeate samples were drawn at regular intervals for AMX analysis as detailed in section 2.2.2. When the experiment was achieved, the feed tank was emptied and filled with distilled water.

Fig. 1 here

2.4. Sequential process EC - NF

The sequential EC – NF process is schematized in Fig. 1. In a first time, several batch EC were performed in order to empty the feed tank of the NF with 6 L of filtered effluent, then the NF was carried out. The rejection of AMX was performed at pH 2.5 and 10 at an optimized current intensity of 0.7 A for the EC and an operating pressure of 0.5 MPa for the NF.

3. Results and discussion

3.1. Use of calcium containing electrolyte

In EC process using aluminum electrodes, the treated solutions are generally supplemented with chloride or nitrate salt of monovalent cations in order to increase their electrolytic conductivity and to destroy the passivating layer on the anode surface. In the

present work, the AMX solutions were supplemented with $Ca(NO_3)_2$. The addition of calcium salt has been rarely applied in water treatment, but it offers some advantages. The addition of $Ca(OH)_2$ has been found to be an efficient coagulant [41,42] and the presence of calcium electrolyte improves EC processes [43-44]. So, in the presence of calcium nitrate, the involvement of calcium in the electrocoagulation process is expected to give improvements.

3.2. Electrolysis behavior

The analysis of solutions during EC, such as pH, electrolytic conductivity and turbidity, give information regarding the physicochemical curse of the process [45,46]. In the presence of chloride or nitrate of monovalent cation the pH increases and reaches values which are depending upon the nature of the co-cations. The variations of pH, electrolytic conductivity and turbidity of solution during EC of AMX solutions in the presence of $Ca(NO_3)_2$ electrolyte are presented in Fig. 2. They show some differences with the published results for monovalent cations [45,46]:

(i) During the first 10 min the turbidity does not increase. This agrees with the slow pH increase which does not allow the precipitation of aluminum hydroxides.

(ii) The pH increase does not reach alkaline value as it was the case for monovalent nitrate which reached a value of 9.5 in the presence of $NaNO_3$ [46]. In the present case, the pH reaches a maximum value about 7.0, after a buffered episode at pH 6.2.

(iii) The electrolytic conductivity notably increases, showing that the electrolysis increases the concentration of ionic species in the solution.

Fig. 2 here

The EC process afforded a sludge in the solution and a deposit on the cathode. These materials were isolated and the results of their analyses are given later (section 3.7).

3.3. Effect of the current intensity on AMX removal

The current intensity is one of the critical parameters that can be controlled directly. The theoretical aluminum concentration C_{Al} (g m^{-3}) is given by Eq. (1) where I is the constant current (A), t is the electrolysis time (s), Mw is the molecular weight of aluminum (27 g mol^{-1}), Z is the chemical equivalence (3 for aluminum), F is the Faraday's constant (96,487 C mol^{-1}) and V is the volume of the reactor (m^3).

$$C_{Al} = \frac{It \ M_w}{ZFV} \quad (1)$$

As a consequence of the increase of the current intensity, the charge loading was increased and led to a better removal of AMX. The influence of current intensity from 0.1 A to 1 A on the removal efficiency of AMX is presented in Fig. 3. As expected, the current increase improves the removal rate of AMX. The rise in the AMX removal efficiency with respect to the increase in current intensity is related to the increased amount of metal hydroxides.

Fig. 3 here

All the possible electrochemical and chemical reactions are given in Eqs. (2-10). The alumina is written as aluminum hydroxide for an easier presentation. As shown previously [45] and with Eqs (4,5) the use of a nitrate electrolyte leads to the formation of hydroxide which is involved in the pH increased, contrary to what is observed in the investigated case in the presence of calcium nitrate. The explanation is due to the chemical reaction of Eq. (7) which consumes hydroxide anion and leads to a cathode deposit of $Ca(OH)_2$. Besides, because this hydroxide consumption, all Al^{3+} ions cannot react, they remain in solution, take the place of Ca^{2+} and this increases the electrolytic conductivity.

Possible electrochemical reactions:

$$\boldsymbol{At\ the\ anode: Al \rightarrow Al^{3+} + 3e^-} \quad \textbf{(2)}$$

$$\textbf{At the cathode}: 3H_2O + 3e^- \rightarrow \frac{3}{2}H_2 + 3OH^- \quad (3)$$

$$NO_3^- + 8e^- + 7H_2O \rightarrow NH_4^+ + 10OH^- \quad (4)$$

$$NO_3^- + 8e^- + 6H_2O \rightarrow NH_3 + 9OH^- \quad (5)$$

Possible chemical reactions:

$$Al^{3+} + 3OH^- \rightarrow Al(OH)_3 \quad (6)$$

$$Ca^{2+} + 2OH^- \rightarrow Ca(OH)_2 \quad (7)$$

Possible balances:

$$\textbf{for } (a)(b) \textbf{and } (e): Al \rightarrow \frac{3}{2}H_2 + Al(OH)_3 \quad (8)$$

$$\textbf{for } (a)(c) \textbf{and } (e): \frac{8}{3}Al + NO_3^- + 7H_2O \rightarrow NH_4^+ + \frac{8}{3}Al(OH)_3 + 2OH^- \quad (9)$$

$$\textbf{for } (a)(d) \textbf{and } (e): \frac{8}{3}Al + NO_3^- + 6H_2O \rightarrow NH_3 + \frac{8}{3}Al(OH)_3 + OH^- \quad (10)$$

3.4. Effect of pH

Amoxicillin is amphoteric in nature and the successive pKa values of 2.68, 7.49 and 9.63 correspond to the ionization of the functional groups -COOH, $-NH_3^+$ and -OH, respectively [47] (Fig. S1). The possible successive structures of AMX may be written AMX^+, $AMX^{\pm}$, AMX^- and AMX^{2-}. Fig. 4A shows a maximum removal efficiency of AMX of 52.7% at the pH value of 3. The removal efficiency decreases to 21% on increasing the pH up to 10. At pH < 3, the decrease in removal efficiency could be associated to the formation of a lower amount of electrogenerated sorbent. The substantial decrease in AMX removal in the range of pH 8 – 10 may be appropriated with the competing nature between – OH groups and AMX^- and AMX^{2-}. The availability of AMX in the form of zwitter ions (as red spheres) in the pH range 3 – 7, get attracted towards the surface of alumina which bears the positively charged species as $AlOOH_2^+$. However, the transformation of AMX as anionic form (as blue spheres) at pH ≥ 8 developed a repulsive effect against the competitive OH^- ions, thus causing the lessened adsorption on to the surface of alumina. The interactive mechanism between AMX ions and the alumina is depicted in Fig. 5.

Fig. 5 here

3.5. Effect of initial AMX concentration

The removal of AMX as a function of initial AMX concentration is shown in Fig. 4B. The removal efficiency of AMX decreased from 74.5% to 19.9% when the concentration increased from 10 mg L^{-1} to 150 mg L^{-1}. This decreasing in the removal efficiency is probably due to the lack of active sites in the metal hydroxide flocs involved in the trapping of an increasing number of AMX molecules. Despite the AMX removal decreasing, the sorption capacity of AMX increased up to 130 mg g^{-1}.

Fig. 6 here

3.6. Adsorption kinetics and isotherms

The equations for kinetic models *viz*., pseudo – first – order [48], pseudo – second – order [49] and Elovich [50] are given by Eqs. (11 – 13), respectively, where q_e and q_t are the adsorbed amounts (mg g^{-1}) at equilibrium and time, t (min^{-1}), respectively, k_1 and k_2 are the pseudo-first-order and pseudo-second-order (g mg^{-1}min) rate constants. 'A' is the initial adsorption rate (mg g^{-1} min^{-1}) and 'B' is the constant of desorption (g mg^{-1}).

$$q_t = q_e(1 - exp^{-k_1.t}) \quad (11)$$

$$q_t = \frac{K_2 {q_e}^2 t}{1 - K_2 q_e t} \quad (12)$$

$$q_t = A + Bln(t) \quad (13)$$

The results are summarized in Table 1 and the kinetic plots are given in Fig. S2A. The kinetic data for the pseudo – first – order model reveals that the rate constant and sorption capacity were increased respectively to five times and 2.83 times to the increase in the initial AMX concentration of 15 times. Up on validating the pseudo – second – order model, the influence of initial AMX concentration on the rate constant (by 5.05 times) and sorption

capacity (by 2.2 times) can be conceived. The rate constants and sorption capacities are directly proportional to the initial AMX concentration with the reasonable fit of the pseudo – first – order and pseudo – second – order models as evident from R^2 values. The initial adsorption rate (A) and the constant of desorption (B) were recorded in the range of 0.0934 – 1.0661 mg $g^{-1}min^{-1}$ and 20.195 – 27.596 respectively. The observed regression coefficient values for higher AMX concentrations of 100 mg L^{-1} and 150 mg L^{-1} in the Elovich model did not fit well with the adsorption system.

Table 1 here

The compliance of isotherm models such as Langmuir (Eq. (15)) [51], Freundlich (Eq. (16)) [52] and Temkin (Eq. (17)) [53] with the present AMX sorption system was studied for various AMX concentrations and the isotherm data and graph are shown in Table 2 and Fig. S2B, respectively.

$$q_e = q_o \frac{K_L C_e}{1 + K_L C_e} \quad (15)$$

$$q_e = K_F C_e^{1/n} \quad (16)$$

$$q_e = \frac{RT}{b_{Te}} \ln(a_{Te} Ce) \quad (17)$$

The sorption capacity is the amount (mg g^{-1}) of AMX at a particular time (q_o) and at equilibrium (q_e), Ce is the residual AMX concentration at equilibrium (mg L^{-1}) and K_L (L mg^{-1}) is the Langmuir isotherm constant. K_F is a measure of the adsorption capacity (mg g^{-1}) and 1/n is the adsorption intensity or surface heterogeneity. The Temkin constants, A_T and B_T are maximum binding energy and isotherm constant respectively. Based on the regression coefficients, firstly, Langmuir model fits appreciably well with 0.968 followed by Temkin model with the value of 0.902. From Langmuir model, the monolayer adsorption capacity (q^o) was 145.46 mg g^{-1} with the constant K_L of 0.116 relating the net enthalpy value (H) of adsorption ($K_L \, \alpha \, e^{-\Delta H/RT}$). Scrupulously, K_L is the reciprocal of concentration at which half

saturation of the adsorbent is attained. The dimensionless constant separation factor, R_L can be defined by Eq. (19)

$$R_L = \frac{1}{1+K_L C_o} \quad (19)$$

For the range of AMX concentrations, the value of 0.77 – 0.07 indicated that the adsorption was favorable as per the R_L value between 0 and 1. Secondly, the fit of Temkin model was validated with the heat of sorption (a_{Te}) and isotherm constant (b_{Te}) of 12.19 and 27.19 respectively. The adsorbent's relative adsorption capacity derived from Freundlich model was 39.13 mg g^{-1} with the constant representing the adsorption intensity or surface heterogeneity of 0.271. Freundlich model did not fit well as evidenced from the R^2 values. Thus, the order of compliance of isotherm models is Langmuir > Temkin > Freundlich, based on the regression coefficient values.

The adsorptive removal of AMX has been carried out with a lot of materials. A recent review [55] gives the maximum adsorption capacities of various adsorbents in the range 1.51-570 mg g^{-1}. With a value of 145.46 mg g^{-1}, the adsorption occurring during EC is not the best but it shows a better efficiency than what was observed for many classical adsorbents.

Table 2 here

3.7. EC process: characterization of electrogenerated solids

EC of AMX solutions led to two kinds of electrogenerated solids: an alumina sludge in suspension which was separated by filtration and a cathode deposit of calcium compounds. These solids were analyzed.

3.7.1. FTIR spectral study

The FTIR patterns of the electrogenerated solids are presented in Fig. S3. The alumina sludge presents notable peaks at 3300 cm^{-1} and 1070 cm^{-1} which are characteristic of alumina [56]. The stretching and bending modes for aliphatic C – H groups could be observed at 2930

cm^{-1} and 1420 cm^{-1} respectively both in the alumina sludge and in the cathode deposit. The carbonyl mode of stretching was observed at 1710 cm^{-1} in the cathode deposit. The shoulder at 1340 cm^{-1} is ascribed to the carbonate peak in the cathode deposit and corroborates the formation of calcium carbonate as a consequence of reaction between $Ca(OH)_2$ and atmospheric CO_2. Peaks appearing at 2350 cm^{-1} and 1260 cm^{-1} indicate the γ (S-H) and $–CH_2$ rocking vibrations respectively. The vibrations in the range 800 – 920 cm^{-1} denoted the presence of $AlOO^-$ group in the cathode deposit. The peak at 735 cm^{-1} corresponds to the bending mode of Al – O group and medium intense assignment around 990 cm^{-1} is ascribed to the possible substitution of surface – OH groups by the counter ions [57]. In accordance with the study on the hydration of calcium aluminates [58], a sharp band with medium intensity around 3760 cm^{-1} corroborated the formation of some calcium aluminate in the cathode deposit.

3.7.2. FE – SEM and XRD studies

The investigated micrographs of the sludge and the cathode deposit are shown in Fig. S4. The surface morphology of the sludge appears as through a bulky and agglomerated mass with unevenly dispersed asymmetric grains of porous nature. Contrary to the sludge, the particles of the cathode deposit seem to be highly heterogeneous with rough surface. The above morphological observations differ from each other in terms of particle size and shape. The observed morphological variation could be significant with respect to the compounds formed during electro-coagulation. Conspicuously, as the cathode deposit contains the mixture of AlOOH (diaspore) and $Ca(OH)_2$ (portlandite), it was different from that of the sludge which contained only AlOOH. However, both the coagulated sediment and the cathode deposit appear as if black tinted due to the sorption of antibiotic fragments of carbon networks. The presence of Al and Ca in the sediment and cathode deposit are shown in Fig. S4 (C – E). The XRD pattern of the sludge formed after electrocoagulation substantiated the

formation of amorphous boehmite AlO(OH) whereas the cathode deposit authenticated a crystalline admixture of Portlandite, $Ca(OH)_2$ and Diaspore, AlO(OH) as shown in Fig. S5. The elemental analysis of the sludge and deposit vindicated the presence of carbon which could arise from the AMX molecule (Fig. S5).

3.7.3. X – Ray Photoelectron Spectroscopy (XPS)

XPS was warried out in the range 0 – 800 eV for the sludge and the cathode deposit. The results are shown in Fig. 5. The major Al (2s) peak appeared at 118.1 eV. The Al (2p) deconvoluted peaks for the sludge at 72.5 eV, 74.6 eV and 76.7 eV ($2p_{3/2}$) and, for the cathode deposit at 72.8 eV (2p) and 74.2 eV ($2p_{3/2}$) are attributed to the presence of AlO(OH) as boehmite (Fig. 5). The surface hydroxyl groups in alumina structure (Al-O-H) appear through the peak transitions (O1s) at 531.5 eV, 531.8 eV and 532.1 eV (Fig. 5) in accordance with the XPS study of major minerals which includes boehmite [59]. The binding energy peaks of Ca observed at 347.4 eV ($3p_{3/2}$) and 351.0 eV ($3p_{1/2}$) to resembled the formation of CaO and $CaCO_3$ respectively in the cathode deposit (Fig. 5). The higher peak intensity at 347.4 eV substantiated the presence of calcium hydroxide (as portlandite) rather than calcium carbonate as supported by the XRD study. Conversely, no such calcium compounds were found in the sludge. The deconvoluted peaks belonging to C1s for the sludge and cathode deposit are shown in Fig. 6. The peaks with binding energy at 284.8 eV (sp^3 – C), 286.0 eV and 288.5 eV corresponding to the respective functional groups C – C, C – O and C = O evidence the separated amoxicillin molecule from the aqueous solution during the EC process. Although the elimination of AMX could be advocated, the difference in peak intensities of C1s clearly indicated the varied proportions of the antibiotic molecule in the sludge and the cathode deposit. The peak intensities of C – C and C – O was higher in the sludge than that of the cathode deposit whereas the deposit exceeded than that of the sludge in the peak intensity of C = O group. The peak intensities illustrated the affinity of AMX

containing C – C and C – O groups towards the sludge was greater in sludge by about 4% and 48% respectively to that of deposit. On the other hand, the unsaturated carbonyl group (C = O) of the AMX molecule developed higher affinity (greater by 48%) with the deposit to that of the sludge.

Fig. 6 here

3.7.4. Thermo-Gravimetric Analysis (TGA)

The TGA results of the sludge and the cathode deposit are shown in Fig. S6. The thermogram of the sludge illustrated the formation of three endotherms at 70°C, 355°C and 503 ˚C. The first endotherm at 70°C revealed the loss of water (also for the cathode deposit) and the second endotherm showing a broad range (320 – 370°C) with a maximum at 355°C demonstrated the loss of interstitial water molecules trapped between AlOOH layers [60]. The third one observed in the range 475 – 510°C belongs to the decomposition of AlOOH (boehmite) to γ – alumina (Al_2O_3) through the dehydration process. On taking the endotherms of cathode deposit, an additional (fourth) endotherm appeared at 710°C denoted the decomposition of $CaCO_3$ with the loss of about 27.3%. A blunt (230°C) and sharp (475°C) endotherms correspond to the loss of surface adsorbed water (dehydration) and diaspore decomposition to alumina respectively.

The exothermic peaks for the oxides of carbon (CO and CO_2) for the sludge appeared between 320°C and 350°C and corroborated the adsorbed AMX with CO_2 generation 1.8 times higher than CO. Similarly, an exothermal broad peak of CO_2 for the cathode deposit (200 – 450°C) witnessed the combustion of organic antibiotic molecule. Conspicuously, a sharp exothermic peak at 700°C was pertinent to the decomposition of calcium carbonate to CaO in the deposit as evidential from XPS study. The shift attributing the decomposition of

chlorhexidine loaded $Ca(OH)_2$ from 350 – 400°C to 450 – 500°C was reported [61] in concordance with the present study. The amount of carbon in the deposit was 4.4 times greater than the sludge. The greater loss of mass in the deposit (45.8%) than the sludge (30%) justified the presence of calcium carbonate which on decomposition leaves the residual mass of 54.2% in the deposits.

3.8. Nano-Filtration (NF) process

3.8.1. Effect of pH

In the NF process, the separation of ions is rather achieved by size exclusion and ion – membrane electrical interactions [62]. The mutual dependence between pH and surface charge of the membrane is rather significant during nano-filtration process. The observed isoelectric point (IEP) of Nanomax-50 at pH 4.5 corroborated that the surface of the membrane becomes positive when pH < IEP and negative when pH > IEP. For the operating pressures (0.1 – 0.5 MPa), the removal of AMX was studied in the range of 56 – 66% at pH 2.5 but got increased with respect to the increase in pH and attained the maximum removal of 95 – 99% at pH 10. The structural behavior of AMX molecule in the solution and the surface charge of the membrane at a particular pH signified the efficiency of AMX rejection. The enhanced rejection of AMX at higher pH values (pH > 7) could be associated due to the anionic forms of AMX (divalent and univalent) which developed a strong electrostatic repulsion between AMX and the membrane. As a result, the membrane permeability decreases with an increase in AMX rejection. The nature of negatively charged surface of Nanomax-50 at pH > 5, confirmed in [63] is in compliance with the AMX removal at higher pH values. It seems to be evident that both the influence of molecular sieve (at lower pH) and Donnan repulsion (at higher pH) mechanisms were dominant during the pH gradation as represented in Fig. 7A. The influence of operating pressure (between pH 2 and pH 10) increases the permeate flux based on the solution – diffusion model. The surface forces

become significant at low pressure but on increasing the pressure from 0.1 M Pa to 0.5 M Pa, the training forces towards the permeate increase due to the increasing velocity in pores with increased retention rate. As a consequence, the permeability of water (solvent) increases rapidly as compared to AMX (solute) and resulting in the increased rejection of AMX.

Fig. 7 here

3.8.2. Effect of AMX concentration

The rejection of AMX at all initial concentrations was proportional to the operating pressure. The rejection percentage decreased on increasing the feed concentration of AMX at the pH of 10.05 as shown in Fig. 7B. This may be attributed to the fact that the ionic strength corresponding to the AMX concentration tends to neutralize the negative charges of the membrane. As a consequence, the electrostatic repulsion decreases and there by facilitates the passing of AMX^{-} (exists at pH > pK_a 9.63) through the membrane with lessened removal efficiency of AMX. However, the training forces governed by the operating pressure increased the permeability of water more than that of AMX with an improved removal of AMX. The layer holds up the transport through the membrane and increased the osmotic pressure. Consequently, the decrease in flux lessened the rejection efficiency of AMX.

3.9. The sequential process

The removal efficiency of AMX by EC and NF processes was 61.46% and 56.03% respectively at the pH value of 2.5 (Fig. 8A). On the other hand, at pH 10, the efficiency was 93.6% for NF which was 24.6 times higher than that of EC. Thus, it could be well inferred that the contribution of either EC or NF seems possible with a maximum AMX rejection but at a particular pH of 2.5 or 10. However, the sequential EC – NF model catered the best efficiency of 98.2% and 97.5% at the pH values of 2.5 and 10 respectively and established the equal prominence at a wider pH range. Based on the initial removal of EC (61.46% at pH

2.5), it was quite construed that the NF was able to reject the remaining 38.54% in the sequential EC – NF process. Conversely, as the removal of AMX was just 3.83% (EC at pH 10), the remaining rejection load of 96.18% by the sequential process was quite high and thus associated with the lessened life time due to the fouling behavior of membranes which is best described by the hydrodynamic and thermodynamic properties of the foulants. In pertinent to the fouling behavior, [64] proved the inverse relationship of the floc size with its thermodynamic interaction on the surface of the membrane. From the practical point of view, the rejection load for the NF segment was comparatively lesser in the sequential process at the pH of 2.5 than at 10. The initial EC process avoided the severe accumulation of AMX on the surface of the membrane or within the pore structure during the secondary treatment with NF and thus the membrane was preserved from fouling. In addition, the formation of larger flocs during the EC process might have minimized the forward transport velocity and the adherence of flocs on the surface of the membrane as well [64]. In favor of the present interest, paper [65] demonstrated the impact of organic contaminants towards the fouling behavior of membranes and the efficient performance of the sequential EC – NF process in the preservation of membranes. Thus, the enhanced removal of AMX in the sequential EC – NF system can best be justified by the predominant effects of EC process in combination with the NF process as that of the hybrid study published in [66,67].

Fig. 8 here

3.10. Electrical energy consumption

The energy consumption for the EC, NF and the EC – NF sequential process was calculated. The energy for EC was calculated by Eq. (20) where E_{EC} is the energy consumption in kWh m^{-3}; V, I, t and v are the voltage (V), the current intensity (A), the time

(h) and the volume (m^3), respectively. The energy consumed for EC was found to be 6.30 kWh m^{-3}.

$$E_{EC} = \frac{VIt}{v} \quad (20)$$

The energy for NF was calculated by Eq. (21) where η_P is the pump efficiency (0.85), Q_P is the permeate flow rate (m h^{-1}), A is the membrane surface (0.37 m^2) and ω_{pump} is the rate of pump work which is equal to $\Delta P \times Q_A$; where ΔP is the pressure applied to the raw feed solution and Q_A is the volumetric feed flow rate (m^3 s^{-1}).

$$E_{NF} = \frac{\omega_{pump}}{Q_p \times \eta_p \times A} \quad (21)$$

Eq. (21) can be rewritten by Eq. (22)

$$E_{NF} = \frac{\Delta P \times Q_A}{Q_p \times \eta_p \times A} \quad (22)$$

From Eq. (22), the electricity consumption was calculated to be 6.10 kWh m^{-3}. For the sequential process, the energy consumption of 8.69 kWh m^{-3} was calculated. The comparison of the electricity consumption of the separate process (EC and NF) and the sequential processes is presented in Fig. 8B. The energy consumed by the sequential process is 30% lower than for the theoretical value of 12.41 kWh m^{-3}. This observed power reduction in the sequential process was achievable due to the lessened electrical energy of about 61% in the NF part with the electricity consumption of 2.39 kWh m^{-3} (against the electricity consumption of 6.1 kWh m^{-3} for NF). As a consequence of pre-treatment using EC, the volumetric feed flow (Q_A) and the permeate flow rate (Q_P) of NF in the sequential process were decreased and thereby causing a reduction in the power consumption.

4. Conclusion

In view of the above results and suitable discussion, the following conclusions can be drawn:

The electrocoagulation process recorded the highest removal of 52.7% at the pH of 3 whereas the NF process established an excellent removal of 99% at pH of 10. The removal efficiency of AMX during the EC process was decreased on increasing the initial AMX concentration. The fit of pseudo – (first and second) – order kinetic models and, Langmuir followed by Temkin isotherm model was well evidenced from the regression coefficient values. The increase in the current intensity (EC process) and the operating pressure (NF process) at the optimized pH values increased the removal of AMX; however, the NF process excelled than the EC process in the percentage efficiency. The XRD patterns for the alumina sediment obtained from the EC process ascertained the presence of boehmite in the sludge with the crystalline admixture of AlOOH (diaspore) and $Ca(OH)_2$ (portlandite) in the cathode deposits. The XPS analysis corroborated the peaks for elements such as Al, Ca, O and C. The CaO peak witnessed by XPS was reconfirmed by the thermal study through the decarboxylation endothermic peak of $CaCO_3$ at 700ºC. The sequential EC – NF process was studied with an excellent AMX removal efficiency of 98.2% and 97.5% at the pH of 2.5 and 10 respectively. Taking the prolonged life of the membrane into consideration, it was accredited that the pH of 2.5 was very effective and efficient towards the treatment of AMX by adopting the sequential process. In line with the electrical energy consumption during the three treatment processes, the sequential process was more favorable with the power reduction by about 30% as compared to the theoretical consumption of 12.411 kWh m^{-3}. In fine, the sequential EC – NF process was very much plausible based on the maximized AMX removal efficiency, minimized electrical energy consumption and the prolonged life of the Nanomax-50 membrane due to the pretreated feed contributed from the EC process. The fate of the resulting sludge after the treatment of EC process is possibly with the scope of

blending it with clay materials for the application of constructions as burnt bricks such that the disposal problem is fairly circumvented.

Credit authorship contribution statement

Aimad Oulebsir: Investigation, Writing original draft. **Toufik Chaabane**: Methodology, Supervision, Writing. **Hanane Tounsi**: Investigation. **Kiyoshi Omine**: Supervision. **Venkataraman Sivasankar**: Writing – review & editing. **Abdenacer Flilissa**: Supervision. **André Darchen**: Writing – review & editing.

Declaration of Competing Interest

The authors declare that they have no known competing financial interest or personal relationship that could have appeared to influence the work reported in this paper.

Acknowledgement

We would like to thank the heads of the collaborating institutes, CNRS, National College of Chemistry (ENSCR, Rennes, France), P.G. and Research Department of Chemistry, Pachaiyappa's College (Chennai, India), Nagasaki University (Nagasaki, Japan), University of Science and Technology Houari Boumédiène (USTHB, Algiers, Algeria).

References

[1] T. Deblonde, C. Cossu-Leguille, P. Hartemann, Emerging pollutants in wastewater: A review of the literature, International J. Hygiene Environ. Health 214 (2011) 442-448, https://doi.org/10.1016/j.ijheh.2011.08.002.

[2] J. Margot, L. Rossi, D.A. Barry, C. Hollinger, A review of the fate of micropollutants in wastewater treatment plants, WIREs Water. 2 (2015) 457-487, https://doi.org/10.1002/wat2.1090.

[3] J. Lalwani, A. Gupta, S. Thatikonda, C. Subrahmanyam, An industrial insight on treatment strategies of the pharmaceutical industry effluent with varying qualitative characteristics, J. Environ. Chem. Eng. 8 (2020) 104190, https://doi.org/10.1016/j.jece.2020.104190.

[4] J. Wang, S. Wang, Removal of pharmaceuticals and personal care products (PPCPs) from wastewater: A review, J. Environ. Manage. 182 (2016) 620-640, https://doi.org/10.1016/j.jenvman.2016.07.049.

[5] M. Taheran, S.K. Brar, M. Verma, R.Y. Surampalli, T.C. Zhang, J.R. Valero, Membrane processes for removal of pharmaceutically active compounds (PhACs) from water and wastewaters, Sci. Total Environ. 547 (2016) 60-77, https://doi.org/10.1016/j.scitotenv.2015.12.139.

[6] I. Sirés, E. Brillas, Remediation of water pollution caused by pharmaceutical residues based on electrochemical separation and degradation technologies: A review, Environ. Int. 40 (2012) 212-229, https://doi.org/10.1016/j.envint.2011.07.012.

[7] S. Garcia-Segura, L.M. Bellotindos, Y.-H. Huang, E. Brillas, M.-C. Lu, Fluidized-bed Fenton process as alternative wastewater treatment technology – A review, J. Taiwan Inst. Chem. Eng. 67 (2016) 211-225, https://doi.org/10.1016/j.jtice.2016.07.021.

[8] H.B. Quesada, A.T.A. Baptista, L.F. Cusioli, D. Seibert, C. de Oliveira Bezerra, R. Bergamasco, Surface water pollution by pharmaceuticals and an alternative of removal by low-cost adsorbents: A review, Chemosphere. 222 (2019) 766-780, https://doi.org/10.1016/j.chemosphere.2019.02.009.

[9] Y.J. Chan, M.F. Chong, C.L. Law, D.G. Hassell, A review on anaerobic-aerobic treatment of industrial and municipal wastewater, Chem. Eng. J. 155 (2009) 1-18, https://doi.org/j.cej.2009.06.041.

[10] O. Ganzenko, D. Huguenot, E.D. van Hullebusch, G. Esposito, M.A. Oturan, Electrochemical advanced oxidation and biological processes for wastewater treatment: a review of the combined approaches, Environ. Sci. Pollut. Res. 21 (2014) 8493-8524, https://doi.org/10.1007/s11356-014-2770-6.

[11] D. Cecconet, D. Molognoni, A. Callegari, A.G. Capodaglio, Biological combination processes for efficient removal of pharmaceutically active compounds from wastewater: A review and future perspectives, J. Environ. Chem. Eng. 5 (2017) 3590-3603, https://doi.org/10.1016/j.jece.2017.07.020.

[12] G.B. Dindas, Y. Caliskan, E.E. Celebi, M. Tekbas, N. Bektas, H.C. Yatmaz, Treatment of pharmaceutical wastewater by combination of electrocoagulation, electro-fenton and photocatalytic oxidation processes, J. Environ. Chem. Eng. 8 (2020) 103777, https://doi.org/10.1016/j.jece.2020.103777.

[13] E. Brillas, I. Sirés, Chapter 11 – Hybrid and sequential chemical and electrochemical processes for water decontamination (Edited by C.A. Martinez-Huitle, M.A. Rodrigo, O. Scialdone) (2018) 267-304, https://doi.org/10.1016/B978-0-12-813160-2.00011-0.

[14] S.X. Zha, Y. Zhou, X. Jin, Z. Chen, The removal of amoxicillin from wastewater using organobentonite, J. Environ. Manage. 129 (2013) 569-576, https://doi.org/10.1016/j.jenvman.2013.08.032

[15] A. Yazidi, M. Atrous, F.E. Soetaredjo, L. Sellaoui, S. Ismadji, A. Erto, A. Bonilla-Petriciolet, G.L. Dotto, A. Ben Lamine, Adsorption of amoxicillin and tetracycline on activated carbon prepared from durian shell in single and binary systems: Experimental study and modeling analysis, Chem. Eng. J. 379 (2020) 122320, https://doi.org/10.1016/j.cej.2019.122320

[16] I. Anastopoulos, I. Pashalidis, A.G. Orfanos, I.D. Manariotis, T. Tatarchuk, L. Sellaoui, A. Bonilla-Petriciolet, A. Mittal, A. Nunez-Delgado, Removal of caffeine, nicotine and

amoxicillin from (waste)waters by various adsorbents. A review, J. Environ. Manage. 261 (2020) 110236, https://doi.org/10.1016/j.jenvman.2020.110236

[17] M.M.H. Guerra, I.O. Alberola, S.M. Rodriguez, A.A. Lopez, A.A. Merino, J.M.Q. Alonso, Oxidation mechanisms of amoxicillin and paracetamol in the photo-Fenton solar process, Water Res. 156 (2019) 232-240, https://doi.org/10.1016/j.watres.2019.02.055

[18] M. Verma, A.K. Haritash, Degradation of amoxicillin by Fenton and Fenton-integrated hybrid oxidation processes, J. Environ. Chem. Eng. 7 (2019) 102886, https://doi.org/10.1016/j.jece.2019.102886

[19] J. Zhao, Y. Sun, F. Wu, M. Shi, X. Liu, Oxidative degradation of amoxicillin in aqueous solution by thermally activated persulfate, Hindawi J. Chem. (2019) article 2505823, https://doi.org/10.1155/2019/2505823

[20] F. Sopaj, M.A. Rodrigo, N. Oturan, F.I. Podvorica, J. Pinson, M.A. Oturan, Influence of the anode materials on the electrochemical oxidation efficiency. Application to oxidative degradation of the pharmaceutical amoxicillin, Chem. Eng. J. 262 (2015) 286-294, https://doi.org/10.1016/j.cej.2014.09.100

[21] Z. Seifollahi, A. Rahbar-Kelishami, Amoxicillin extraction from aqueous solution by emulsion liquid membranes using response surface methodology, Chem. Eng. Technol. 42 (2019) 156-166, https://doi.org/10.1002/ceat.201800089

[22] D. Dimitrakopoulou, I. Rethemiotaki, Z. Frontistis, N.P. Xekoukoulotakis, D. Venieri, D. Mantzavinos, Degradation, mineralization and antibiotic inactivation of amoxicillin by UV-A/TiO_2 photocatalysis, J. Environ. Manage. 98 (2012) 168-174, https://doi.org/10.1016/j.jenvman.2012.01.010

[23] A. Shahtalebi, M.H. Sarrafzadeh, M.M.M. Rahmati, Application of nanofiltration membrane in the separation of amoxicillin from pharmaceutical wastewater, Iran J. Environ. Health Sci. Eng. 8 (2011) 109-116.

[24] F.J. Benitez, J.L. Acero, F.J. Real, G. Roldan, E. Rodriguez, Ultrafiltration and nanofiltration membranes applied to the removal of the pharmaceuticals amoxicillin, naproxen, metoprolol and phenacetin from water, J. Chem. Technol. Biotechnol. 86 (2011) 858-866, https://doi.org/10.1002/jctb.2600

[25] A. Moarefian, H.A. Golestani, H. Bahmanpour, Removal of amoxicillin from wastewater by self-made polyethersulfone membrane using nanofiltration, J. Environ. Health Sci. Eng. 12 (2014) 127, https://doi.org/10.1186/s40201-014-0127-1

[26] R. Kidak, S. Dogan, Medium-high frequency ultrasound and ozone based advanced oxidation for amoxicillin removal in water, Ultrasonics Sonochemistry, 40 (2018) 131-139, https://doi.org/10.1016/j.ultsonch.2017.01.033

[27] M. Li, Z. Zeng, Y. Li, M. Arowo, J. Chen, H. Meng, L. Shao, Treatment of amoxicillin by O_3/Fenton process in a rotating packed bed, J. Environ. Manage. 150 (2015) 404-411, https://doi.org/10.1016/j.jenvman.2014.12.019

[28] V. Homem, A. Alves, L. Santos, Microwave-assisted Fenton's oxidation of amoxicillin, Chem. Eng. J. 220 (2013) 35-44, https://doi.org/10.1016/j.cej.2013.01.047

[29] A. Mojiri, M. Vakili, H. Farraji, S.Q. Aziz, Combined ozone oxidation process and adsorption methods for the removal of acetaminophen and amoxicillin from aqueous solution; kinetic and optimization, Environ. Technol. Innovation 15 (2019) 100404, https://doi.org/10.1016/j.eti.2019.100404

[30] B.G. Padilla-Robles, A. Alonso, S.A. Martinez-Delgadillo, M. Gonzalez-Brambila, U.J. Jauregui-Haza, J. Ramirez-Munoz, Electrochemical degradation of amoxicillin in aqueous media, Chem. Eng. Process. 94 (2015) 93-98, https://doi.org/10.1016/j.cep.2014.12.007

[31] H. Alidadi, A. Ghorbanian, M. Ghorbanian, E. Rahmanzadeh, N. Nemanifar, M. Mehrabpour, Evaluation of amoxicillin antibiotic removal by electrocoagulation process from aqueous solutions: optimization through response surface methodology, Desalination Water Treatment, 132 (2018) 350-358, https://doi.org/10.5004/dwt.2018.23159

[32] J. Chatterjee, N. Rai, S.K. Sar, Kinetic isotherm of amoxicillin antibiotic through adsorption and its removal by electrocoagulation, Oriental J. Chem. 30 (2014) 775-784, https://doi.org/10.13005/ojc/300251

[33] D. Balarak, K. Chandrika, M. Attaolahi, Assessment of effective operational parameters on removal of amoxicillin from synthetic wastewater using electrocoagulation process, J. Pharmaceut. Res. Internat. 29 (2019) 1-8, https://doi.org/10.9734/jpri/2019/v29i130227

[34] H. Zhang, Q. He, J. Luo, Y. Wan, S.B. Darling, Sharpening nanofiltration: Strategies for enhanced membrane selectivity, ACS Appl. Mater. Interfaces (2020), https://doi.org/10.1021/acsami.0c11136

[35] S. Chellam, M.A. Sari, Aluminum electrocoagulation as pretreatment during microfiltration of surface water containing NOM: A review of fouling, NOM, DBP, and virus control, J. Hazard. Mater. 304 (2016) 490-501, https://doi.org/10.1016/j.jhazmat.2015.10.054[

[36] N.P. Gamage, S. Chellam, Aluminum electrocoagulation pretreatment reduces fouling during water microfiltration, J. Membrane Sci. 379 (2011) 97-105, https://doi.org/10.1016/j.memsci.2011.05.051

[37] I.S. Kim, N. Jang, The effect of calcium on the membrane biofouling in the membrane bioreactor (MBR), Water Res. 40 (2006) 2756-2764, https://doi.org/10.1016/j.watres.2006.03.036

[38] M.R. Mehrnia, H. Azami, M.H. Sarrafzadeh, Fouling mitigation in membrane bioreactors using multivalent cations, Colloids Surf. B: Biointerfaces 109 (2013) 90-96, https://doi.org/10.1016/j.colsurfb.2013.03.009

[39] H. Zhang, J. Xia, Y. Yang, Z. Wang, F. Yang, Mechanism of calcium mitigating membrane fouling in submerged membrane bioreactors, J. Environ. Sci. 21 (2009) 1066-1073, https://doi.org/10.1016/S1001-0742(08)62383-9

[40] H. Sano, K. Omine, M. Prabhakaran, A. Darchen, V. Sivasankar, Groundwater fluoride removal using modified mesoporous dung carbon and the impact of hydrogen-carbonate in borehole samples, Ecotoxicol. Environ. Safety, 165 (2018) 232-242, https://doi.org/10.1016/j.ecoenv.2018.09.001

[41] Y. Fu, D.D.L. Chung, Coagulation of oil in water using sawdust, bentonite and calcium hydroxide to form floating sheets, Applied Clay Sci. 53 (2011) 634-641, https://doi.org/10.1016/j.clay.2011.05.014

[42] A. Hamdani, M. Mountadar, O. Assobhei, Comparative study of the efficacy of three coagulants in treating dairy factory waste water, Internat. J. Dairy Technol. 58 (2005) 83-88, https://doi.org/10.1111/j.1471-0307.2005.00198.x

[43] C.-Y. Hu, S.-L. Lo, W.-H. Kuan, High concentration of arsenate removal by electrocoagulation with calcium, Separ. Purif. Technol. 126 (2014) 7-14, https://doi.org/10.1016/j.seppur.2014.02.015

[44] S.R. Tchamango, K.W. Ngayo, P.D.B. Belibi, F. Nkouam, M.B. Ngassoum, Treatment of a dairy effluent by classical electrocoagulation and indirect electrocoagulation with aluminum electrodes, Separ. Sci. Technol. (2020), https://doi.org/10.1080/01496395.2020.1748889

[45] I. Mishima, M. Hama, Y. Tabata, J. Nakajima, Improvement of phosphorous removal by calcium addition in the iron electrocoagulation process, Water Sci. Technol. 76 (2017) 920-927, https://doi.org/10.2166/wst.2017.256

[46] E. Tchomgui-Kamga, N. Audebrand, A. Darchen, Effect of co-existing ions during the preparation of alumina by electrolysis with aluminum soluble electrodes: Structure and defluoridation activity of electro-synthesized adsorbents, J. Hazard. Mater. 254-255 (2013) 125-133, https://doi.org/10.1016/j.jhazmat.2013.03.044

[47] S. Zaidi, V. Sivasankar, T. Chaabane, V. Alonzo, K. Omine, R. Maachi, A. Darchen, Preparation and characterizations of thermally regenerable electro-generated adsorbents (EGAs) for a competitor electrocoagulation process, J. Taiwan Inst. Chem. Eng. 97 (2019) 272-279, https://doi.org/10.1016/j.jtice.2019.02.009

[48] O. Pezoti, A.L. Cazetta, K.C. Bedin, L.S. Souza, A.C. Martins, T.L. Silva, O.O. Santos Júnior, J.V. Visentainer, V.C. Almeida, NaOH-activated carbon of high surface area produced from guava seeds as a high-efficiency adsorbent for amoxicillin removal: Kinetic, isotherm and thermodynamic studies. Chem. Eng. J. 288 (2016) 778–788, https://doi.org/10.1016/j.cej.2015.12.042

[49] S. Lagergren, Zur theorie der sogenannten adsorption geloster stoffe, Kungliga Svenska Vetenskapsakademiens, Handligar 24 (1898) 1–39, https://doi.org/10.4236/ajac.2013.45028

[50] Y.S. Ho, Second-order-kinetic model for the sorption of cadmium onto tree fern: a comparison of linear and non-linear methods, Water Res. 40 (2006) 119–125, https://doi.org/10.1016/j.watres.2005.10.040

[51] C. Aharoni, F.C. Tompkins, Kinetics of adsorption and desorption and the Elovich Equation. Advance in catalysis and related subjects, Academic Press, New York, 1970, https://doi.org/10.1016/S0360-0564(08)60563-5

[52] I. Langmuir, The constitution and fundamental properties of solids and liquids, J. Am. Chem. Soc. 38 (1916) 2221–2295, https://doi.org/10.1021/ja02268a002

[53] H.M.F. Freundlich, Uber die adsorption in losungen, Z. Phys. Chem. 57A (1906) 385–470, https://doi.org/10.1515/zpch-1907-5723

[54] M.J. Temkin, V. Pyzhev, Recent modifications to Langmuir isotherms, Acta Physiochim. USSR 12 (1940) 217–222.

[55] I. Anastopoulos, I. Pashalidis, A.G. Orfanos, I.D. Manariotis, T. Tatarchuk, L. Sellaoui, A. Bonilla-Petriciolet, A. Mittal, A. Nunez-Delgado, Removal of caffeine, nicotine and amoxicillin from (waste)waters by various adsorbents. A review, J. Environ. Management, 261 (2020) 110236, https://doi.org/10.1016/j.jenvman.2020.110236

[56] E. Kumar, A. Bhatnagar, U. Kumar, M. Sillanpaa, Defluoridation from aqueous solutions by nano – alumina: Characterization and sorption studies, J. Hazard. Mater. 186 (2011) 1042 – 1049, https://doi.org/10.1016/j.jhazmat.2010.11.102

[57] R. Liu, W. Gong, H. Lan, Y. Gao, H. Liu, J. Qu, Defluoridation by freshly prepared aluminium hydroxides, Chem. Eng. J. 175 (2011) 144 – 149, https://doi.org/10.1016/j.cej.2011.09.083

[58] D. Torrens – Martin, L. Fernandez – Carrasco, S. Martinez – Ramirez, Hydration of calcium aluminates and calcium sulfo aluminate studied by Raman Spectroscopy, Cement Concrete Res. 47 (2013) 43 – 50, https://doi.org/10.1016/j.cemconres.2013.01.015

[59] J.T. Kloprogge, L.V. Duong, B.J. Wood, R.L. Frost, XPS study of the major minerals in bauxite: Gibbsite, bayerite and (pseudo-) boehmite, J Colloid Interface Sci 296 (2006)572 – 576, https://doi.org/10.1016/j.jcis.2005.09.054

[60] S. Zanganesh, A. Kajbafvala, N. Zanganesh, M.S. Mohajerani, A. Lak, M.R. Bayati, H.R. Zargar, S.K. Sadrnezhaad, Self – assembly of boehmite nanopetals to form 3D high surface area nano architectures, Appl. Phys. A 99 (2010) 317 – 321, https://doi.org/10.1007/s00339-009-5534-2

[61] B.M. Priyadarshini, T.S. Subramanian, N. Karthikeyan, A.S. Fawsy, Characterization of chlorhexidine – loaded calcium – hydroxide micro particles as a potential dental pulp-capping material, Bioengineering 4 (2017) 59, https://doi.org/10.3390/bioengineering4030059

[62] K. Linde, A.S. Jonsson, Nanofiltration of salt solutions and landfill leachate, Desalination 103 (1995) 223 – 232, https://doi.org/10.1016/0011-9164(95)00075-5

[63] A. Abidi, N. Gherraf, L. Segni, M. Rabiller-Baudry, B.Tidjani, Effect of operating parameters on the selectivity of nano-filtration phosphates transfer through a Nanomax-50 membrane, Arab. J. Chem. 9 (2016) S334 – S341, https://doi.org/10.1016/j.arabjc.2011.04.014

[64] H. Hong, W. Peng, M. Zhang, J. Cheng, Y. He, F. Wang, X. Weng, H. Yu, H. Lin, Thermodynamic analysis of membrane fouling in a submerged membrane bioreactor and its implications, Bioresour. Technol. 146 (2013) 7–14, https://doi.org/10.1016/j.biortech.2013.07.040

[65] T. Marian, L.D. Nghiem, Landfill leachate treatment using hybrid coagulation – nanofiltration process, Desalination 250 (2010) 677 – 681, https://doi.org/10.1016/j.desal.2009.03.024

[66] M. Hosseinzadeh, G.N. Bidhendi, A. Torabian, N. Mehrdadi, M. Pourabdullah, A new flat sheet membrane bioreactor hybrid system for advanced treatment of effluent, reverse osmosis pretreatment and fouling mitigation, Bioresour. Technol. 192 (2015) 177–184, https://doi.org/10.1016/j.biortech.2015.05.066

[67] B.M.B. Ensano, L. Borea, V. Naddeo, M.D.G. de Luna, V. Belgiorno, Control of emerging contaminants by the combination of electrochemical processes and membrane bioreactors, Env. Sci. Poll. Res. 26 (2019) 1103 – 1112, https://doi.org/10.1007/s11356-017-9097-z

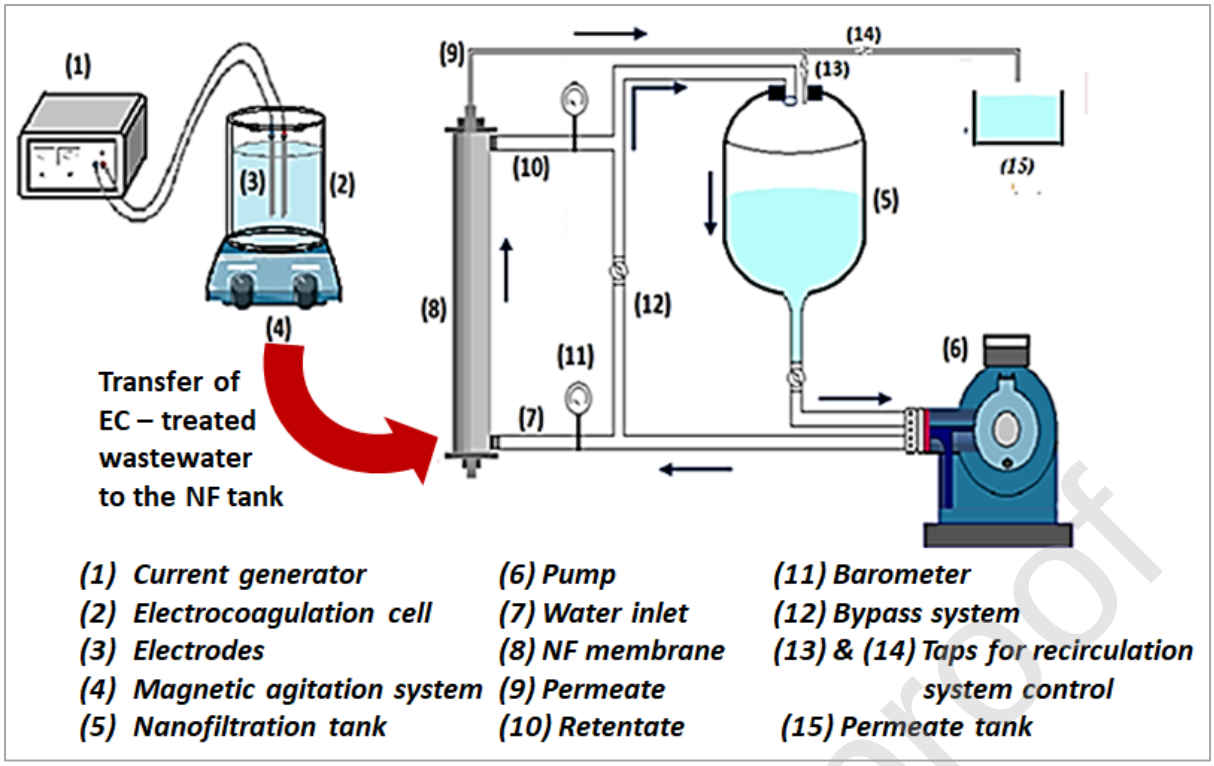

Fig. 1. Schematic diagram of sequential EC – NF process

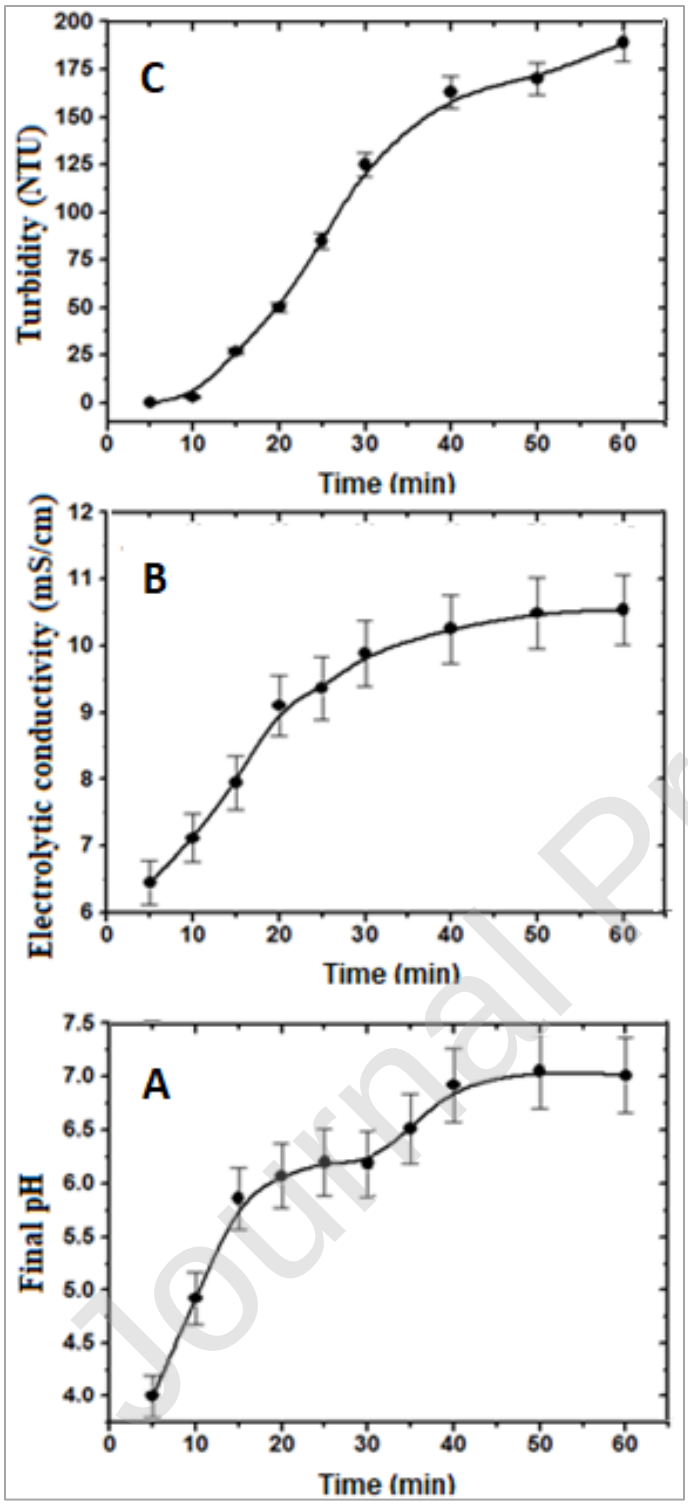

Fig. 2. Variations of pH and electrolytic conductivity (A), and turbidity (B) during EC (Specific conditions: AMX concentration: 50 mg/L; Electrolyte 1 L of 12.19 mM $Ca(NO_3)_2$; Temperature: 300 K; Current intensity: 0.7 A; Distance between the electrodes: 1 cm).

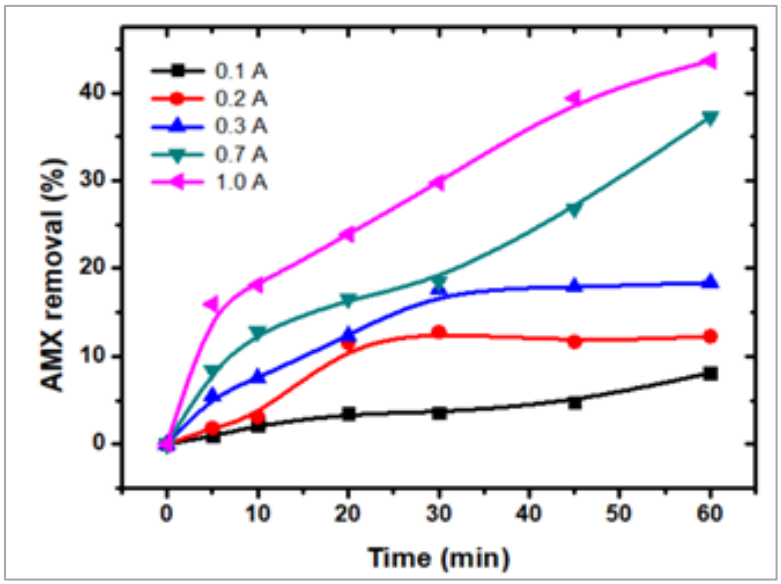

Fig. 3. Effect of current intensity on the variation of AMX removal (Specific conditions: AMX concentration: 50 mg/L; pH: 5.5; distance between the electrodes: 1 cm)

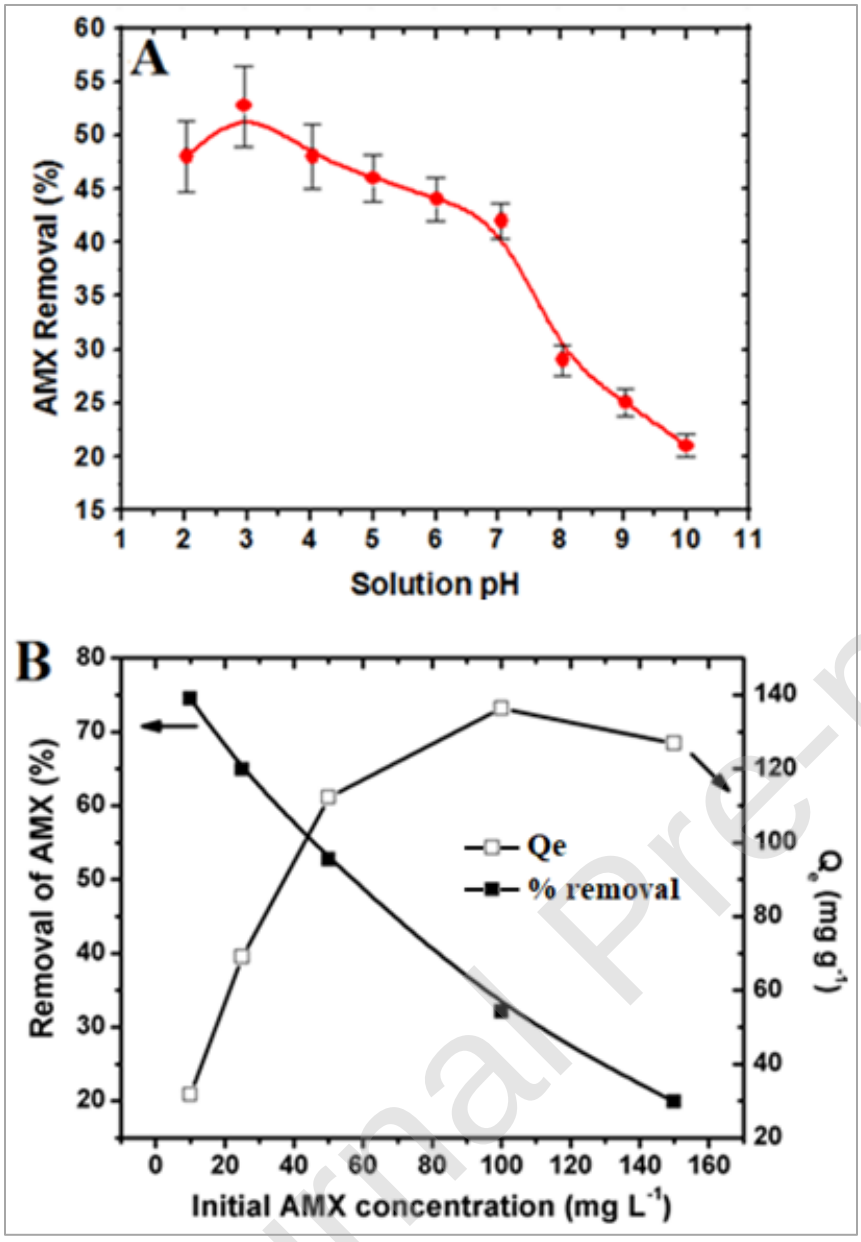

Fig. 4. Influence of initial pH (A) and initial AMX concentration (B) on the AMX removal and on the removed quantity Qe during the EC process (Time of EC: 60 min; Distance between the electrodes: 1 cm. Specific conditions for (A): AMX concentration: 50 mg/L; Current intensity: 0.7 A; Specific conditions for (B): initial pH :2.5; Current intensity :0.7 A)

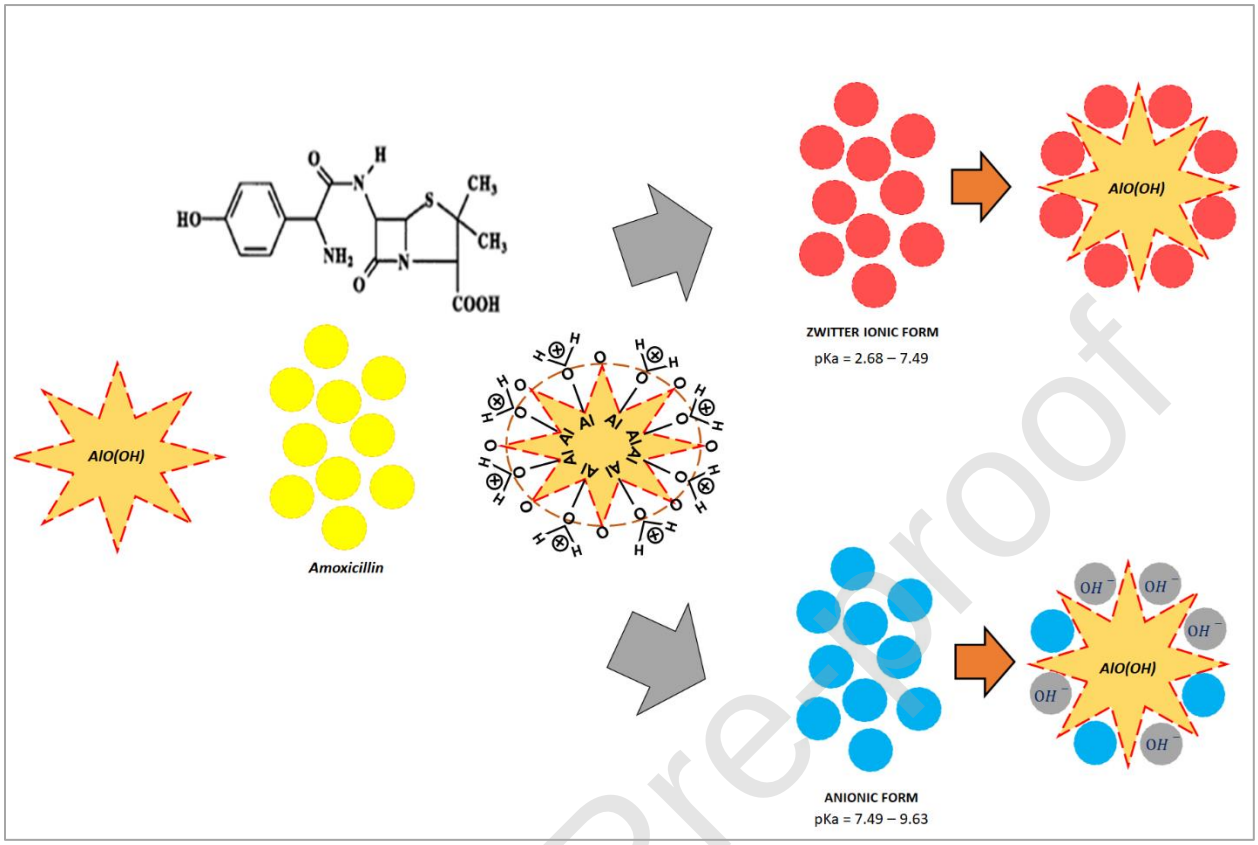

Fig. 5. Mechanism of the adsorption of AMX onto the electro-generated alumina

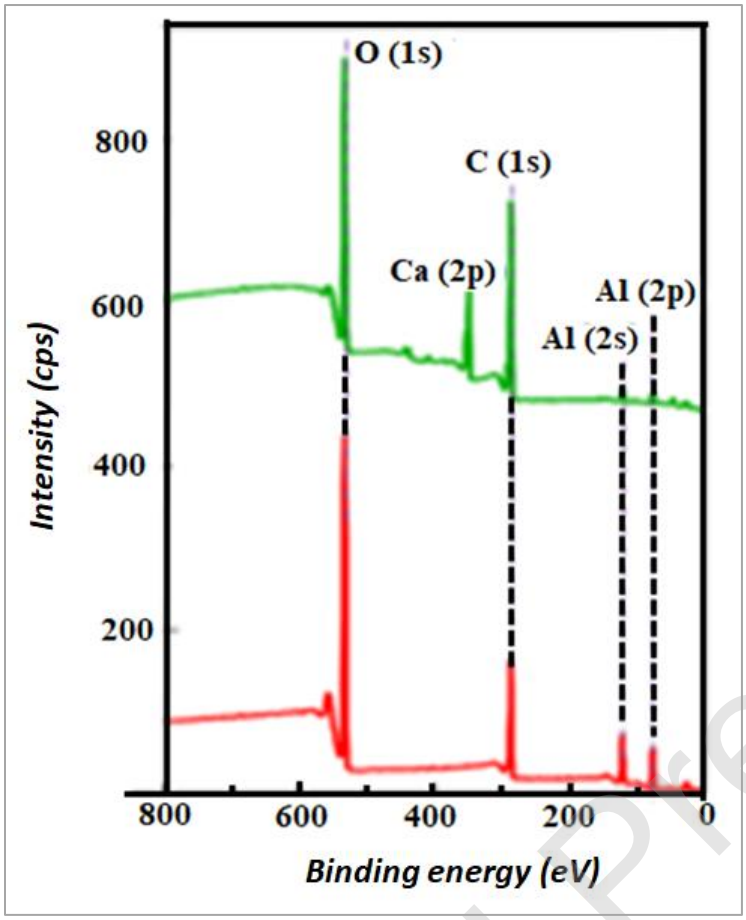

Fig. 6. X – ray Photoelectron spectra of electrogenerated amoxicillin – alumina sludge (red line) and cathode deposit (green line).

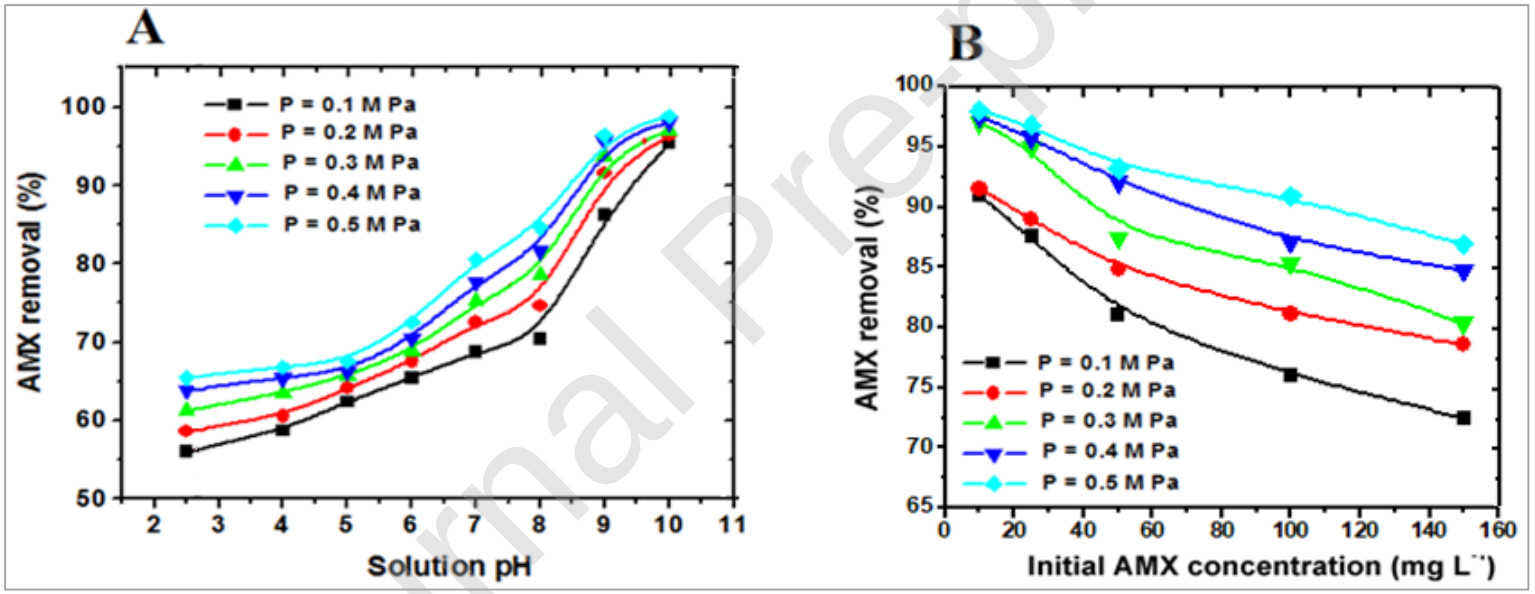

Fig. 7. Effect of pH (A) and AMX concentration (B) on the AMX removal during the NF process (The operating pressures are given on the figures. Specific conditions: (A) Initial AMX concentration: 25 mg/L; (B) pH: 10).

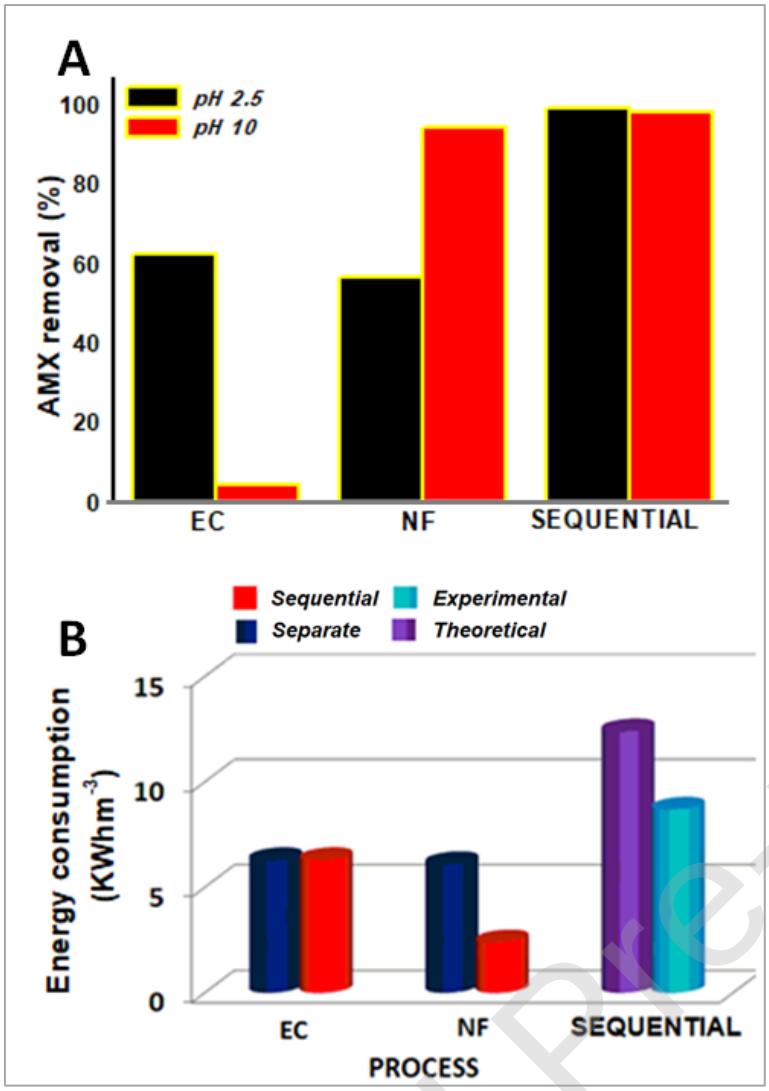

Fig. 8. Effect of pH on AMX removal efficiency (A) and energy consumption (B) during EC, NF and EC – NF sequential process (Specific conditions: (EC) current intensity: 0.7A; Time of EC: 60 min; Distance between the electrodes: 1cm; pH: 2.5; (NF) pH: 10; Pressure: 0.5 M Pa).

Table 1 Effect of contact time on AMX removal by electrocoagulation (EC)

Models	Parameters	Initial AMX concentration (mg L^{-1})				
		10	**25**	**50**	**100**	**150**
Pseudo-first order	Q_e	63.225	84.736	122.640	143.861	178.950
	K_1	0.050	0.076	0.115	0.186	0.251
	R^2	0.959	0.948	0.966	0.967	0.872
Pseudo-second order	Q_e	86.799	104.732	141.958	156.800	191.309
	K_1	0.471	0.753	1.010	1.900	2.380
	R^2	0.935	0.921	0.966	0.893	0.951
Elovich	A	0.2360	0.0935	0.1839	0.6591	1.0661
	B	21.022	23.964	27.596	21.150	20.195
	R^2	0.951	0.896	0.918	0.721	0.851

Table 2 Effect of initial concentration of AMX removed by electrocoagulation (EC)

Models	Parameter	Value
Langmuir	q^o (mg g^{-1})	145.464
	K	0.116
	R^2	0.968
Freundlich	K_F (mg g^{-1})	39.13
	1/n	0.271
	R^2	0.791
Temkin	a_{Te}	12.199
	b_{Te}	27.19
	R^2	0.902